To be presented at the 1st International Induction Heat Treating Symposium, September 16-18, 1997, Indianapolis, Indiana.



# TORO II Simulations of Induction Heating in Ferromagnetic Materials

Douglas R. Adkins, David K. Gartling, J. Bruce Kelley, Philip M. Kahle
Sandia National Laboratories, P.O. Box 5800
Albuquerque, NM 87185-0835
(505) 844-0611



## Abstract

TORO II is a finite element computer program that is used in the simulation of electric and magnetic fields. This code, which was developed at Sandia National Laboratories, has been coupled with a finite element thermal code, COYOTE II, to predict temperature profiles in inductively heated parts. The development of an effective technique to account for the nonlinear behavior of the magnetic permeability in ferromagnetic parts is one of the more difficult aspects of solving induction heating problems. In the TORO II code, nonlinear, spatially varying magnetic permeability is approximated by an effective permeability on an element-by-element basis that effectively provides the same energy deposition that is produced when the true permeability is used. This approximation has been found to give an accurate estimate of the volumetric heating distribution in the part, and predicted temperature distributions have been experimentally verified using a medium carbon steel and a 10kW industrial induction heating unit. Work on the model was funded through a Cooperative Research and Development Agreement (CRADA) between the Department of Energy and General Motors' Delphi Saginaw Steering Systems.

INDUCTION HARDENING is extensively used because it is a very fast, energy-efficient, in-line heat treating technology that applies energy only to the volume of material required to be hardened. Short treatment times and decreased distortion generally result in less scrap, rework, and post-heat-treatment machining of parts. Induction hardening is also an environmentally benign process, requiring no endothermic atmospheres, plating processes, or stripping tanks. In contrast, the primary competing heat treating technology, carburizing, is an off-line batch process in which the entire volume of material is heated in a furnace. Batch heat treating results in higher direct energy costs, longer manufacturing lead times, and greater amounts of distortion when parts are quenched [Storm and Chaplin, 1987]. In today's competitive environment, the ability to heat treat parts rapidly with in-line technology generates significant savings and quality improvements.

Despite the advantages of induction hardening, its broad application is hampered by the limited design tools that are available to predict the outcome of induction heating processes. Coil designs, the selection of induction power supplies, and the development of heating schedules are largely experience-based and heavily dependent on iterative procedures. Because of this trial-and-error aspect of the induction system design, tooling and process development are not often optimized. One of the goals of the current collaborative program is to improve capabilities to model the inductive heating process.

In the classical treatment of induction heating problems, the depth of resistive (or joule) heating in a part is assumed to be proportional to the depth of penetration of the magnetic field (Davies and Simpson, 1979). The magnetic field decreases exponentially with distance into the part, and, at a skin depth of

$$\delta = \sqrt{2\rho/\mu\omega},$$

the magnetic field is about 37% of what it is at the surface. In this expression, $\rho$ is the material density, $\mu$ is magnetic permeability, and $\omega$ is the driving frequency of the magnetic field. At high frequencies, the skin depth can be on the order of a few tenths of a millimeter, so it is often assumed that the power is applied only to the surface, and that heating of the interior of the part is a result of thermal conduction alone.

This simple treatment of induction heating can provide useful insights into relationship between the dominant material and process parameters, but the simplicity also obscures many complicated aspects of the induction heating process. For instance, the permeability in

## DISCLAIMER

ferromagnetic materials can vary by three orders of magnitude during a single cycle of the magnetic field. Similarly, both the resistivity and the magnetic permeability are functions of temperature, and, as the part heats up, the magnetic field will penetrate deeper.

A full solution of the equations that describe the induction heating process in thick steel plates has been provided by Lim and Hammond (1970). In arriving at their solution, they consider the nonlinear behavior of the permeability as it is manifested in the relationship between the magnetic field strength, $\vec{H}$, and the magnetic flux density, $\vec{B}$. To solve the problem in this fashion, however, it is necessary to march through time with a time step much smaller than the period of the driving magnetic field. Even though the solution does become periodic after an initial transient, the solution process is slow.

Labridis and Dokopoulos (1989) found that by using a time harmonic approach to solving Maxwell's equations, they could reduce computational times by a factor of 12, and still predict joule heating fluxes that differed by less than 2% from Lim and Hammond's solution for a semi-infinite slab. To obtain their harmonic solution, Labridis and Dokopoulos assumed that the permeability is constant with respect to time, but varies spatially in the material. The effective, time-invariant permeability is a weighted average of the non-linear permeability in an idealized material subjected to the same magnetic fields. (This is similar to the concept of magnetic coenergy that is used to determine the force in electromagnets [Plonsey and Collin, 1961, pp. 290-297].) Our current work builds Labridis and Dokopoulos approach, and extends it to two-dimensional geometries, and systems where the electromagnetic and thermal properties change during the induction heating process. The TORO II code also determines all of the magnetic fields using the current in the coil as the driving input.

## Model Development

The induction heating model consists of two codes that are linked through the Parallel Virtual Machine (PVM) software package. The thermal problem is solved by the COYOTE II code and the electromagnetic problem, as described by Maxwell's equations, is solved by the TORO II code. COYOTE II is fully described in a report by Gartling and Hogan [1994], and the theoretical background and computational users manual of TORO II is presented in a two-volume set by Gartling [1996].

For induction heating systems, Maxwell's equation can be written in the current driven form,

$$\vec{\nabla} x \left( \frac{1}{\mu} \vec{\nabla} x \vec{A} \right) = -\sigma \frac{\partial \vec{A}}{\partial t} + \vec{J}_S \qquad (1)$$

where $\vec{A}$ is the magnetic vector potential and $\vec{J}_S$ is the current flux through the coil. This expression, together with the current continuity equation,

$$\vec{\nabla} \cdot \left( -\sigma \frac{\partial \vec{A}}{\partial t} - \sigma \vec{\nabla} \phi \right) = 0 \; . \qquad (2)$$

are used to solve for $\vec{A}$ and the electric scalar potential, $\phi$.

Knowing these potentials, the magnetic flux density can be determined through the expression,

$$\vec{B} = \vec{\nabla} x \vec{A} \qquad (3)$$

and the electric field strength can be obtained by the expression

$$\vec{E} = -\frac{\partial \vec{A}}{\partial t} - \vec{\nabla} \phi \qquad (4)$$

Likewise, the current density in the material is simply

$$\vec{J} = \sigma \vec{E} \, , \qquad (5)$$

and the Joule heating (or eddy current heating) in the part is given by the expression

$$JOULE\ HEATING = \left| \vec{E} \right| \left| \vec{J} \right| = \frac{\left| \vec{J} \right|^2}{\sigma} \; . \qquad (6)$$

Basically, TORO II solves the electromagnetic problem to determine the Joule heating and the magnitude of the magnetic flux density. The Joule heating is used as a source term in the thermal model of the system which is governed by Fourier's equation

$$\rho C \frac{\partial T}{\partial t} = \nabla \cdot \left( k \nabla T \right) + \left| \vec{E} \right| \left| \vec{J} \right| + losses \, . \qquad (7)$$

What is referred to as *losses* in this expression is the hysteretic losses in the material. These losses are determined by the material properties and the magnitude of the magnetic flux density, $B \equiv \left| \vec{B} \right|$.

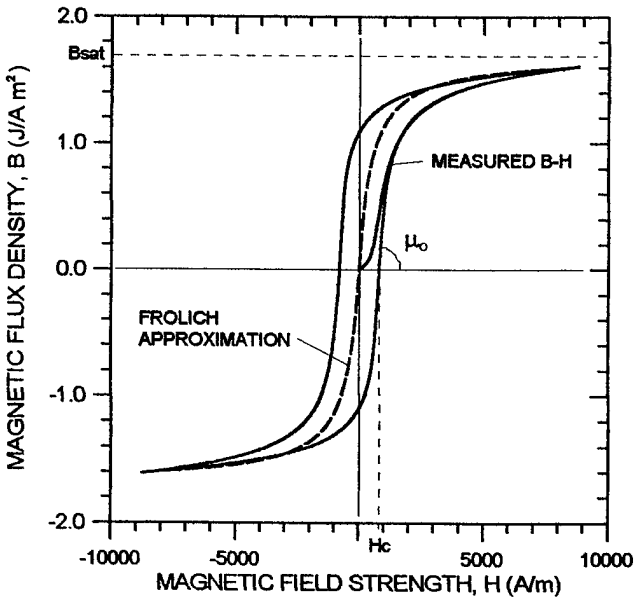


$$B = \frac{H}{(\alpha + \beta|H|)} = \frac{(1-\beta|B|)}{\alpha} H, \quad \alpha = \frac{1}{\mu_o}, \quad \beta = \frac{\mu_o - \mu_\infty}{\mu_o B_{sat}}$$

Fig. 1 - Measured *B-H* curve for 1050M steel at room temperature and the Frolich representation used in deriving the equivalent permeability.

Equations 1-7 are the basic equations that are solved in the induction heating model. One complicating factor in obtaining a solution, however, is the dependence of the magnetic permeability, $\mu$, in Equation 1 on the magnitude of the magnetic flux density, *B*. Ferromagnetic materials exhibit the relationship between *B* and the magnitude of the magnetic field strength, *H*, that is illustrated in Figure 1; $\mu$ is the slope of this curve. Over the course of one cycle of the induced magnetic field, this slope can vary by more than three orders of magnitude for most common steels. In effect, the magnitude of $\mu$ will determine how far the magnetic field penetrates into the part, and this will in turn determine the depth that the eddy current heating penetrates the part. It is possible to use TORO II to solve the electromagnetic equations using the relationship between *B* and *H* illustrated in Figure 1, but such an approach would be too slow for practical applications since the hysteresis loop is traversed for each cycle of the applied electromagnetic field.

Following the approach of Labridis and Dokopoulos [1989], the effective permeability was chosen to match the energy density defined by the *B-H* curve using the expression

$$W = \int_0^B H \, dB \, . \tag{8}$$

The exact *B-H* curve is first replaced with a modified Frolich approximation that is illustrated in Figure 1 and the energy density is calculated as

$$W = -\frac{\alpha B}{\beta} - \frac{\alpha}{\beta^2} \ln(1-\beta B) \, . \tag{9}$$

The constants $\alpha$ and $\beta$ are defined in Figure 1. For an idealized material with a constant permeability, the energy density is

$$W = \frac{1}{2\,\mu_{eff}} B^2 \, . \tag{10}$$

Combining equations 9 and 10 gives the following expression for the effective permeability;

$$\mu_{eff} = \frac{-\beta^2 B^2}{2\alpha\left[\beta B + \ln(1-\beta B)\right]}, \qquad |B| \le B_{sat} \, . \tag{11}$$

Similarly, when the magnetic flux density in the part exceeds the saturation level (which is typical in induction heating processes), the effective permeability is

$$\mu_{eff} = \frac{-\beta^2 B^2}{2\alpha\left[\beta B + \ln(1-\beta B) - \frac{\mu_0}{\mu_\infty}\beta^2\left(B^2 - B_{sat}^2\right)\right]}, \; B_{sat} < |B| \tag{12}$$

Since $\mu_{eff}$ is a function of *B*, the EM problem must be solved in an iterative fashion. TORO II first solves equations 1 and 2 using a constant permeability throughout the part, and then, using equations 11 and 12, the effective permeability is determined for each element. Through successive iterations the permeability is updated until the magnetic potentials converge. Based on the TORO II results, COYOTE II determines the temperature profile in the part. In subsequent calculations by TORO II, the temperature profiles calculated by COYOTE II are used to update the material properties and the initial effective permeability profile is based on the previous values at convergence.

## Model Results

Predictions of the model were compared with measured results from a 24-mm diameter by 25.4-mm long solid steel cylinder in a 25.4-mm diameter solenoid coil provided by Delphi Saginaw Steering Systems. A schematic for the steel part in the induction coil, and the corresponding axisymmetric finite element mesh is shown in Figure 2. Electromagnetic fields are propagated through space, so it is necessary to include the surroundings in the mesh. For the current problem, the air was included to about 3.5 diameters beyond the surface of the part. (This distance was found to be

sufficient to remove the influence of the far-field boundary condition on the solution.) Along the edge of the meshing boundary, the magnetic vector potential, $\vec{A}$, was set equal to zero. The current flux density in the coil was the driving input for the model and it was assumed that the current was uniformly distributed in the copper coil. In the model, the cross-sectional area of the coil is 3.08 $cm^2$.

The test specimen was made of a medium carbon steel that is commonly used for induction heat treating. Purdue University's Thermal Physical Properties Lab performed property measurements on the material and the results are illustrated in Figure 3. Magnetization (*B-H*) curves at various temperatures were obtained from KJS Associates in Dayton OH. The measured *B-H* curve at room temperature was previously illustrated in Figure 1, and a list of magnetization parameters that were derived from the KJS measurements are given in Table 1

For the induction model, B-H properties must be known up to the Curie temperature of the test material, which for this steel is 770°C. Above 350°C, however, the electrical insulation on the specimen tested by KJS Associates began to break down. It was therefore necessary to use a theoretical model of $B_{sat}$ as a function of temperature. Based on a theory of ferromagnetism that was proposed by Weiss in 1907 [Plonsey and Collin, 1961, pp. 260-264], the saturation flux density is assumed to behave as

$$\frac{B_{sat}}{B_{sat,rt}} = \tanh\left(\frac{B_{sat}}{B_{sat,rt}}\frac{T_{curie}}{T}\right), \qquad T \le T_{curie} \qquad (13)$$

where $B_{sat,rt}$ is the magnetic flux density at room temperature (=1.69 J/$Am^2$) and $T_{curie}$ is the Curie temperature in degrees Kelvin. Above the Curie temperature, it was assumed that the relative permeability is not a function of temperature.

The validation tests were performed using a 10 kW induction hardening machine furnished by Delphi Saginaw Steering Systems. For this particular unit, the driving current in the coil is generated by discharging a tank circuit at roughly 4 kHz, so the current profile exhibits a ringing pulse followed by a dead-time period. This feature is illustrated as the solid line in Figure 4. The measured cycle frequency for the model validation test was 3780 Hz and the ringing frequency was 7630 Hz.

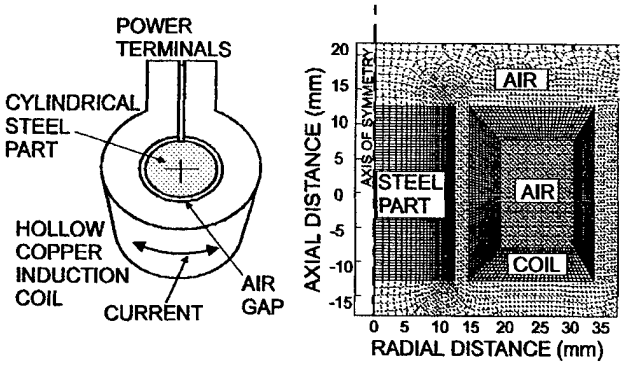


Fig. 2 - Schematic of the steel test specimen in a copper induction coil, and the corresponding finite-element representation. To capture the electromagnetic-scale effects, elements near the surface of the steel part were on the order of 0.1-mm thick.

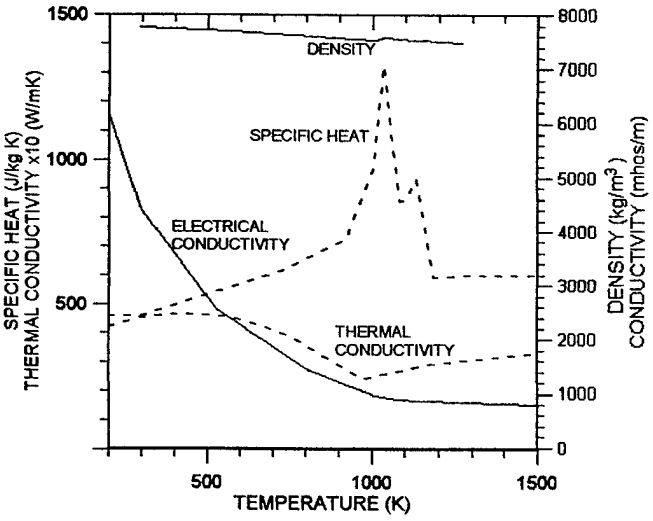


Fig. 3 - Measured thermal and electrical properties of 1050M steel.

TABLE 1. Magnetization properties of the medium carbon steel test specimen.*

| Temperature (°C) | $B_{sat}$ (J/A $m^2$) | $H_c$ (A/m) | $\mu_r$ | $\alpha$ ($A^2m/J$) | $\beta$ (A $m^2$/J) |
|---|---|---|---|---|---|
| 25 | 1.69 | 802 | 2714 | 293.2 | 0.590 |

* Properties are based on measurements made by KJS Associates in Dayton, OH.
$\mu_r$ is the relative permeability, and $\alpha$ and $\beta$ are coefficients in the Frolich approximation.

Since the induction code presently provides solutions for harmonic waveforms, adjustments had to be made to compensate for the true, non-sinusoidal current profile. For the test case, it was assumed that the current frequency was 7630 Hz, however, the volumetric heating (joule and hysteresis losses) for each element was reduced by the ratio of the dead-time to the total cycle-time. The approximated waveform is shown as the broken line in Figure 4. Heating contributed by the dotted section of the driving current is not included in the model.

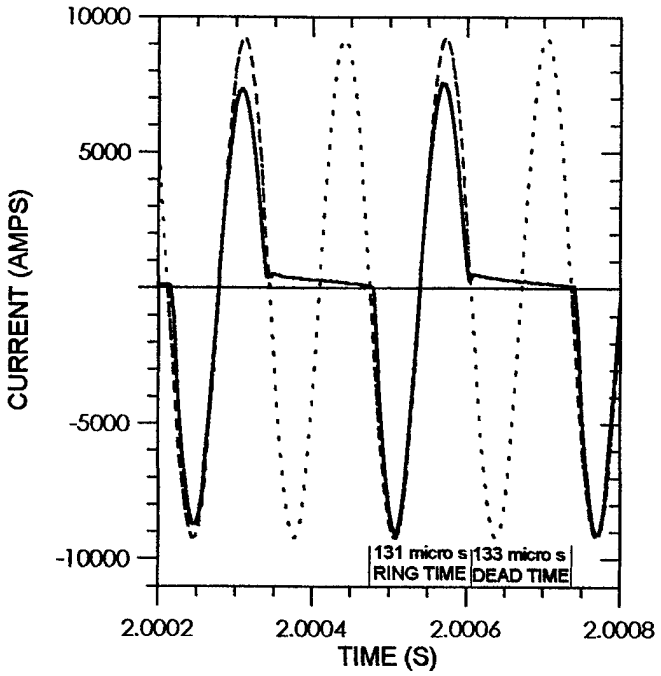


Fig. 4 - Measured current waveform for the test case (solid line). Effective waveform used in the induction model (broken line). The heating contribution of the dotted portion was not included.

In the model validation test, the part was heated for 5.4 seconds before a spray quench was applied to the surface. Predicted temperature contours at the mid-plane of the part are shown in Figure 5. In the early stages of heating, the temperature distribution exhibits a characteristic parabolic profile. Near the surface of the part, however, the temperature profile flattens; this flat region extends deeper into the part as the temperature increases. The flattening of the temperature profile near the surface of the part indicates that heating is occurring deeper in the part as the temperature rises. As Figure 6 illustrates, the maximum heating occurs in the interior of the part in the later stages of heating.

A comparison between the predicted and measured results is provided in Figure 7. Temperatures were measured with 4 thermocouples embedded into the midplane of the test specimen. The intrinsic thermocouples were spot welded into holes at the center, 1/3 radius, and 2/3 radius. The fourth thermocouple was brought diagonally through the wall of the part, and spot welded to the surface. Both the model and the measurements show that the temperature on the surface begins to rise immediately after power is applied to the coil. Heating slows as the temperature approaches the Curie temperature. At about 5.4 seconds into the run, the surface

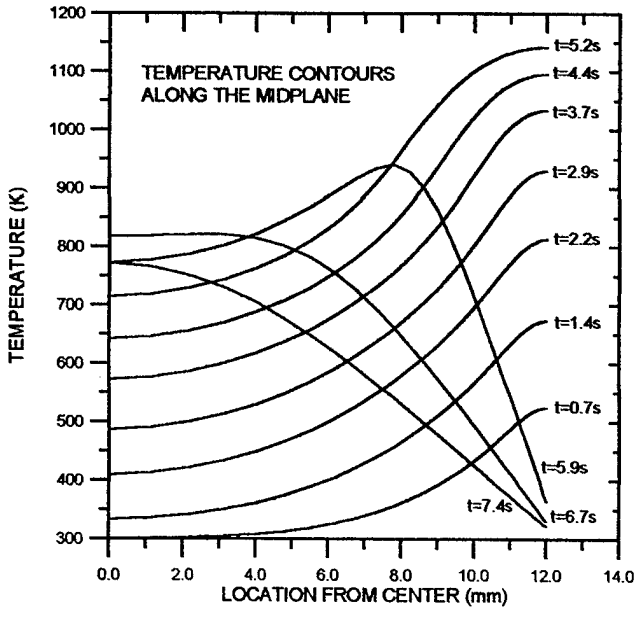


Fig. 5 - Predicted temperature contours in a 25.4-mm long, 24-mm diameter cylinder of 1050 M steel that was heated in a 25.4-mm long, 25.4-mm diameter induction coil. Heating lasted 5.4 seconds and a spray quench immediately followed.

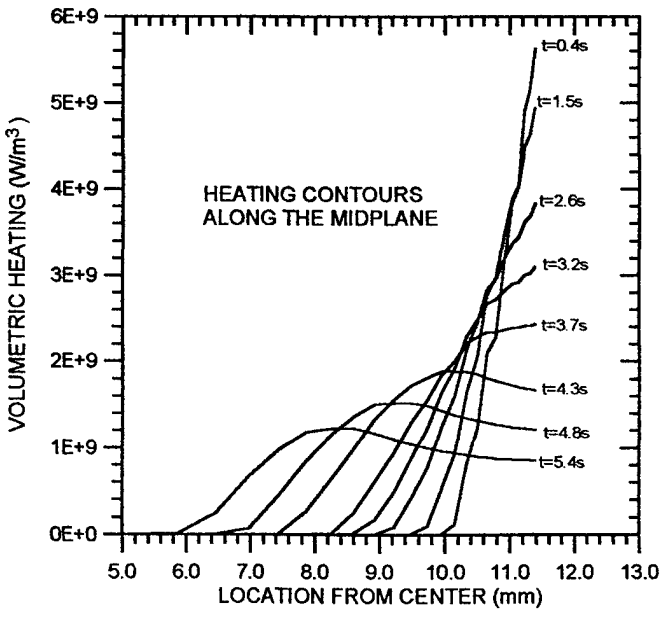


Fig. 6.- Predicted volumetric at the midplane of a 25.4-mm long, 24-mm diameter cylinder of 1050 M steel that was heated in a 25.4-mm long, 25.4-mm diameter induction coil.

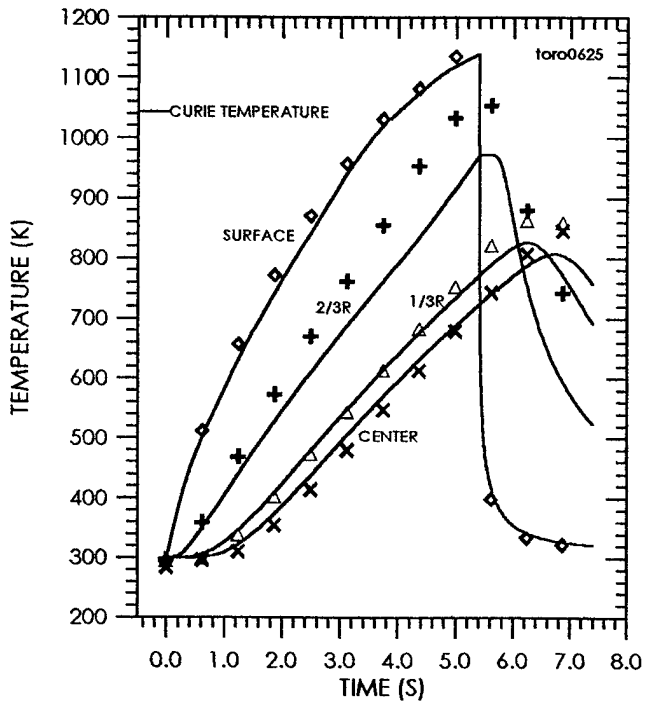


Fig. 7 - Predicted and measured temperatures at the center, 1/3 radius, 2/3 radius, and the surface of the part.

temperature drops rapidly as quenching begins. In the interior of the part, temperatures still rise as thermal energy is conducted inward.

The agreement between the experiment data and the model predictions is quite good at the surface and at the two center-most thermocouples. At the 2/3 radius location (4-mm from the surface), however, the predicted temperatures lag the measured temperatures. Part of this discrepancy might be attributed to the accuracy of locating the thermocouple in the part. As Figure 5 illustrates, temperature gradients are large between 2 to 4 mm beneath the surface of the part; a 1-mm error in the placement of the thermocouple could make a 50°C error in the reported temperature.

While it is possible that a misplacement of the 2/3R thermocouple could cause the discrepancy between measured and predicted temperatures, it is more likely that the measured temperature is correct. Figure 7 shows that the measured temperatures at the center and at 1/3R rise higher than the predicted temperatures after the quench begins. This suggests that the model is under-predicting the amount of thermal energy that is stored in the part. The added energy would likely be reflected as higher temperatures beneath the surface of the part, and, upon quenching, this energy would be conducted into the interior.

The induction model showed that increasing $B_{sat}$ reduces the rate that the surface temperature rises. For materials with a lower value of saturation magnetic flux density, the magnetic field penetrates deeper into the part and the accompanying eddy currents cause heating to occur deeper into the part. Energy from the coil is transferred more efficiently to the part.

The sensitivity of the induction heating process to $B_{sat}$ may offer an explanation to the higher-than-predicted temperatures measured at 2/3R. In the relationship presented in Equation 13, $B_{sat}$ initially decreases only slightly as the temperature increases. If, in reality, $B_{sat}$ decreases more rapidly as temperature increases, then heating would be delivered deeper into the part and the predicted temperature at 2/3R would rise more rapidly. Less of an impact would be seen at the surface because, as Figure 5 illustrates, the temperature contours become flatter near the surface as heating progresses. Of course, this reasoning remains speculative at this time. Efforts are now underway to obtain magnetization curves at higher temperatures.

## Summary and Conclusions

The TORO II code solves a harmonic form of Maxwell's equations to determine the energy that is transferred to parts in an induction heating process. An effective permeability distribution in the part is determined by using an energy weighted average of the true, non-linear magnetization properties of ferromagnetic materials. With this approximation, the model shows that the area of maximum heating moves to the interior of part as the Curie temperature is exceeded near the surface.

Predicted temperature profiles were experimentally verified for a 24-mm diameter, cylindrical part in a circular coil. The predicted temperatures matched well with the validation experiment; however, a discrepancy was evident about 4 mm beneath the surface of the part. This discrepancy indicates that energy is delivered deeper into the part than the model predicts. It is possible that the discrepancy is related to the assumed behavior of the saturation magnetic flux density with temperature. This uncertainty will be resolved when magnetization curves are measured for temperatures up to the Curie temperature of the material.

At this time, additional validation tests are planned for a wide variety of two-dimensional axisymmetric parts. Features such as boot-grooves, tapers and step-changes in shafts will be investigated. The induction code is now functional for solving fully three-dimensional problems, but computational times are excessive. Parts of the code are being reformulated to reduce the time required for three-dimensional solutions.

## Acknowledgments

The authors would like to thank Sharlene McLane, Ron Hoppe, and Jim Farago at Delphi Saginaw Steering Systems for providing parts, an induction machine, and lots of advice. We would also like to thank Russ Skocypec at Sandia and Dave Hitz at Delphi Saginaw Steering Systems for helping

allocate the money for this project. Tony
Robino, Gerald Knorovski and Polly Hop
acknowledged for their practical insig
electromagnetics, materials and code operati
work was performed at Sandia National
supported by the U. S. Department of Energy
number DE-AC04-94AL85000, through a labo
research and development contract.
SC92/01133, SAND97-****C

## References

Davies, J., and Simpson, P., 1979, *Induction He*
*Handbook*, pp. 310-311, McGraw-Hill, London.

Gartling, D. K., and Hogan, R. E., 1994, "COYO
Finite Element Computer Program for Nonlinear
Conduction Problems, Part II, Users Manual," SA
1179, Sandia National Laboratories, Albuquerque

Gartling, D. K., 1996, "TORO II - A Finite Eleme
Computer Program for Nonlinear Quasi-Static Pro
Electrodymanics, Part I, Theoretical Background,"
2472, Sandia National Laboratories, Albuquerque,

Gartling, D. K., 1996, "TORO II - A Finite Elemen
Computer Program for Nonlinear Quasi-Static Prob
Electrodymanics, Part II, User's Manual," SAND96
Sandia National Laboratories, Albuquerque, NM.

Labridis, D., and Dokopoulos, P., 1989, "Calculation
Current Losses in Nonlinear Ferromagnetic Material
*Transactions on Magnetic*, Vol. 25, No. 3, pp. 2665-

Lim, K. K., and Hammond, P., 1970, "Universal Loss
for the Calculation of Eddy-Current Losses in Thick S
Plates," *Proc. Inst. Elec. Eng.*, Vol. 117, pp. 857-864.

Plonsey, R., and Collin, R. E., 1961, Principles and
Applications of Electromagnetic Fields, McGraw-Hill,
York, NY.

Storm, J. M., and Chaplin, M. R., 1987, "Induction Ge
Hardening by the Dual Frequency Method," *Heat Treat*
Vol. 19, No. 6, pp. 30-35.

## Nomeclature

= magnetic vector potential [T m = J/Am]
= magnetic flux density [T = J/Am$^2$]
= magnitude of $\vec{B}$
= saturation magnetic flux density [J/Am$^2$]
= $B_{sat}$ at room temperature [J/Am$^2$]
= specific heat [J/kg K]
= electric field strength [V/m]
= magnetic field strength [A/m]
= coercive magnetic field strength [A/m]
= current flux [A/m$^2$]
= temperature [K]
= Curie temperature [K]
= elemental energy density [J/m$^3$]

= thermal conductivity [W/mK]

= Frolich constant [A$^2$m/J]
= Frolich constant [Am$^2$/J]
= heating skin depth [m]
= driving frequency [radian/s]
= density [kg/m$^3$]
= electrical conductivity [mho/m]
= electric scalar potential [V]
= magnetic permeability [H/m=J/A$^2$m]
= free space permeability = $4\pi x10^{-7}$ H/m
= maximum magnetic permeability [H/m]
= relative permeability $\equiv \mu_o/\mu_\infty$ [H/m]

Report Number (14) SAND--97-0013C
CONF-970982--

Publ. Date (11) 199709
Sponsor Code (18) DOE/DP, XF
UC Category (19) UC-700, DOE/ER

DOE